AIAA JOURNAL
Vol. 36, No. 3, March 1998

Flow Transition in Swirled Liquid Sheets

K. Ramamurthi* and T. J. Tharakan†
Liquid Propulsion Systems Centre, Trivandrum 695 547, India

Experiments are conducted to study the tulip-shaped and cone-shaped liquid sheets formed in swirl nozzles. It is shown that waves rapidly grow on the cone-shaped sheets and lead to its rupture unlike in the tulip-shaped sheets. The transition from the tulip-shaped to the cone-shaped sheet occurs when the liquid phase Weber number of the swirled annular sheet exceeds about 150. The turbulence level in the liquid sheet does not influence the Weber number at which the transition of the shape of the sheet takes place. The frequencies and rate of growth of the waves on the liquid sheets increase with Weber number. The transition takes place when the growth rate of waves is significant. The predicted variations of frequencies and growth rates, obtained by linear perturbation of the axial momentum equation, reproduce the increasing trends with Weber number observed in the experiments; however, the values are higher than those measured. A linear bifurcation analysis brings out the role of the different parameters influencing the stability of the swirled liquid sheet. The annular sheet is seen to be inherently unstable. The existence of a threshold value of Weber number, above which the transition of the shape of swirled liquid sheet takes place, is seen to be valid for all swirled liquid sheets.

Nomenclature

A = matrix defined by Eq. (26)
Ap = flow area in swirler, m^2
C_D = aerodynamic drag coefficient
Cd = coefficient of discharge
Cp = pressure coefficient defined as $P/(\rho u^2)$
$Cp_{g,u}$ = pressure coefficient on upper interface in gas phase
$Cp_{l,u}$ = pressure coefficient on upper interface in liquid phase
D = drag force given by $C_D[\rho u^2/2]$
dL = elemental length of liquid sheet, m
do = orifice diameter, m
ds = mean diameter of swirler, m
F = frequency, Hz
F_1 = meridian component of centrifugal force, N
F_2 = whirl component of centrifugal force, N
f = function defined by Eq. (22)
g = function defined by Eq. (23)
H = nondimensional liquid sheet thickness
h = dimensional sheet thickness, m
I = inertial force on element, N
K_v = flow correction for discharge coefficient
L = distance along sheet, m
N = nondimensional complex frequency
Ns = swirl number defined by Eq. (1)
P = pressure, Pa
R = radius of curvature along the meridian, m
Ra = average surface roughness, μm
Re_l = Reynolds number defined in Eq. (4)
r = radius of liquid sheet, m
r_0 = radius of orifice, m
S_w = ratio of tangential to axial velocities
T = nondimensional time
T_1 = surface tension force due to radius r of sheet, N
T_2 = surface tension force due to radius R along meridian, N
tr A = trace of matrix A
U = nondimensional axial velocity, u/u_0
u = axial velocity of liquid sheet, m/s
u_0 = axial velocity at exit of orifice, m/s
V = nondimensional velocity normal to the liquid sheet
v = velocity normal to liquid sheet, m/s
v_w = tangential velocity, m/s
W = nondimensional wave number defined in Eq. (12)
We_l = Weber number based on the half-thickness of the liquid sheet
We_s = swirl Weber number of liquid sheet
X = nondimensional distance along x axis
x = coordinate along the longitudinal axis of the sheet
y = coordinate normal to the longitudinal axis of sheet
Z = parameter containing Weber number and wave number defined in Eq. (12)
α = angle of sheet with respect to X axis at exit from orifice, deg
β = fraction of air core in the liquid due to swirling liquid
η = disturbance amplitude
η_0 = initial amplitude of the disturbance
θ = angle subtended by the element of the sheet at the axis, rad
λ = wavelength, m
μ = liquid viscosity, Ns/m^2
ξ = nondimensional distance, L/r_0
ρ = density ratio
ρ_g = ambient gas density, kg/m^3
ρ_l = liquid density, kg/m^3
σ = surface tension coefficient, N/m
ϕ = angle of sheet with X axis at any distance L, deg
ψ = helix angle of the swirler, deg

Subscripts

l = liquid
0 = orifice exit condition

Superscripts

$'$ = perturbation quantities
$*$ = stationary point

Received May 12, 1997; presented as Paper 97-1779 at the AIAA 28th Fluid Dynamics Conference, Snowmass Village, CO, June 29–July 2, 1997; revision received Oct. 31, 1997; accepted for publication Nov. 9, 1997.

*Head, Propulsion Research and Studies Group. Associate Fellow AIAA.
†Engineer, Propulsion Research and Studies Group.

Introduction

SWIRLED liquid sheets are often employed in liquid propellant rockets to obtain good atomization and efficient mixing of fuel and oxidizer. The droplets formed from the disintegration of swirled liquid sheets are, in general, smaller than those formed in straight cylindrical jets. The spatial distribution of the droplets obtained with the swirled sheets can be controlled by varying the swirl velocities. The coaxial swirl nozzles, which form such liquid sheets, offer scope for improving the combustion efficiency of the liquid propellant rockets. Some of the existing designs of injection nozzles

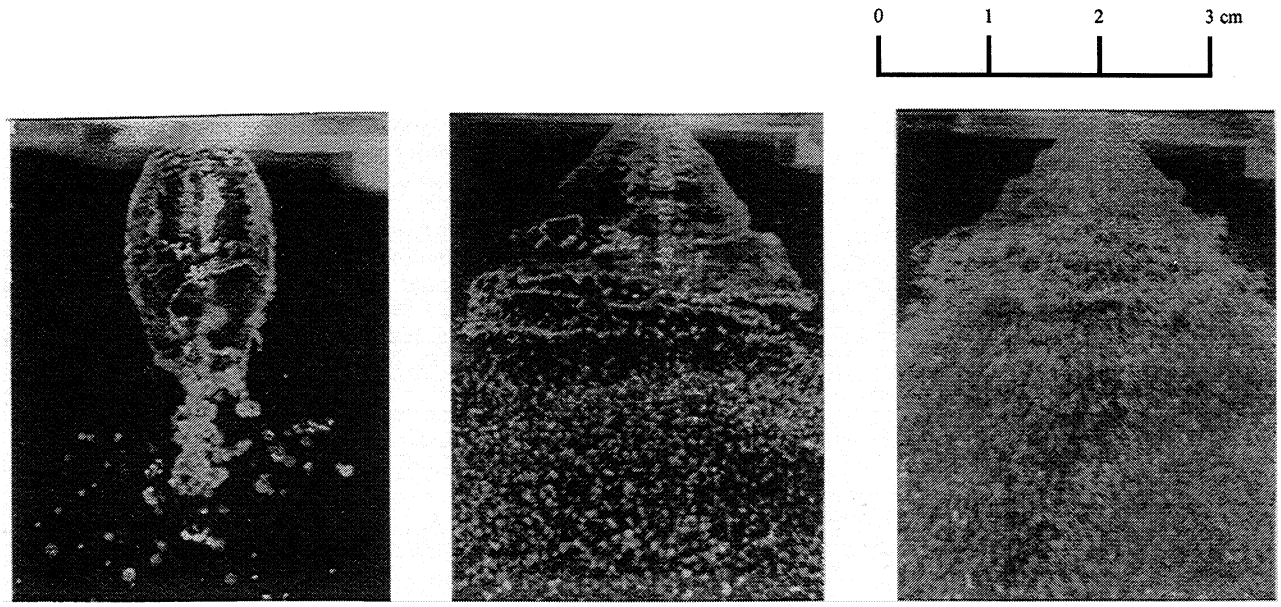

a) Tulip shape b) Transition to cone shape c) Cone shape

Fig. 1 Shape of swirled liquid sheets.

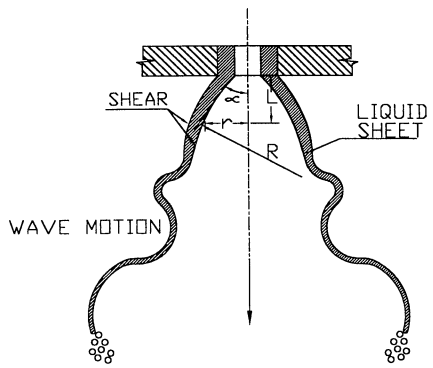

Fig. 2 Schematic of swirled liquid sheet.

do improvise swirl, typical examples being the liquid oxygen elements of cryogenic propellant injectors and the centrifugal injection elements used with hypergolic propellant combinations.

A number of investigations have been carried out on coaxial swirled liquid sheets.[1,2] These have shown the existence of two forms of liquid sheets comprising either a collapsed bulbous shape (tuliplike) or a diverging conical shape. The flow processes contributing to the formation of either of the two shapes and the stability and the disintegration of these two characteristic types of sheets are not clear. The evolution of the swirled liquid sheet issuing from a cylindrical orifice of 3 mm diameter at different injection velocities is shown in Fig. 1. A bulbous tulip-shaped sheet, without any significant wave motion over it, is formed at the lower range of injection velocities of about 2.5 m/s (Fig. 1a). It transits into a cone-shaped diverging sheet at intermediate values of injection velocity of 7.3 m/s and is shown in Fig. 1b. Waves rapidly grow on its surface and lead to the rupture of the sheet. As the injection velocities are further increased, the wavy nature becomes more pronounced and is shown in Fig. 1c for an injection velocity of 16.6 m/s.

Figure 2 gives the flow phenomenon associated with the formation and disintegration of the coaxial swirled liquid sheets. The liquid is injected with axial and tangential velocity components through the orifice to form an annular liquid sheet of radius r at a given distance from the orifice with a radius of curvature R along the meridian axis. The tangential velocity provides centrifugal forces along the radius r, whereas the axial velocity gives centrifugal force normal to the sheet. These centrifugal forces cause the liquid sheets to diverge at the exit of the injection orifice. The surface tension forces from the two radii of curvature r and R act in a direction opposite to the outward centrifugal forces and aid the liquid sheet to collapse. The boundary between the liquid sheet and the environment (high-velocity gas flow or high-pressure gases or ambient atmosphere) is the primary shear flow region. The shear forces at the interface contribute to the growth of disturbances or waves on the liquid sheet.[3,4] The deformation of the liquid sheet, by these disturbances and the turbulence, brings about a change of the surface tension and centrifugal forces and leads to a change in the shape of the sheet.

The factors that lead to the tulip-shaped sheet changing into the cone-shaped sheet, as the injection velocity is increased, are of interest as these findings can be incorporated in the design of swirl nozzles. The effect of turbulence in the flow on the sheet shape and disintegration has been hypothesized to be very influential[5]; however, no specific experimental or theoretical verification has been done by varying the turbulence intensities and the scales of turbulence.

The two characteristic shapes of swirled liquid sheets formed by coaxial swirl injection elements are investigated. A series of experiments is conducted in quiescent atmosphere by varying the injection orifice diameters and swirl numbers. A stability analysis is carried out for the growth of disturbances in the liquid sheet with a view to explain the experimental observations of the different regimes of sheet shape.

Experiments

Coaxial swirled liquid sheets are generated in the quiescent atmosphere using swirl nozzles with different orifice diameters. A schematic of the swirl nozzle is shown in Fig. 3. It comprises a helical swirler of diameter ds with four start rectangular flow passages of total cross-sectional area Ap. The swirl intensities are varied by changing the helix angle ψ, the dimensions of the flow path Ap, and the orifice diameter do. The intensity of swirl is quantified in terms of a swirl number Ns and is defined in terms of the geometrical dimensions of the helical swirler and orifice as[6]

$$Ns = \pi dods \cos\psi/(4\,Ap) \tag{1}$$

The dimensions of swirl nozzles used in the experiments and the range of swirl numbers is given in Table 1. The helical angle of the swirler is varied between 13 and 23 deg. The swirl intensity is changed tenfold by varying the ratio of the diameter of the swirler and the diameter of the orifice and the flow area in the swirler as shown. The swirl numbers obtained are between 1.4 and 14.5.

Experiments are done with distilled water as the test liquid to determine the shape, the surface texture, and the formation of waves in the swirled sheets at different injection pressures. The experimental apparatus is shown schematically in Fig. 4. Water is pressurized with nitrogen gas in a run tank to 1.6 MPa. It is admitted in the swirl

Table 1 Configuration of swirl nozzles

Swirler configuration			Orifice	
Outer diameter, mm	Helix angle, deg	Flow area, mm^2	diameter, mm	Swirl number
6	21	0.6	1	6.4
6	22	1.04	1	3.6
6	23	2.4	1	1.4
8	17	4.5	3	3.3
8	17	6.16	3	2.35
12	13	5.84	4	6
12	13	5.84	6	8.7
12	13	5.84	10	14.5

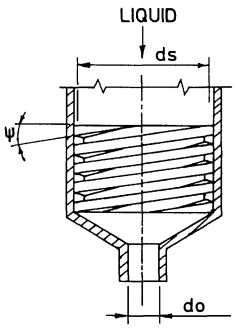

Fig. 3 Swirl nozzle.

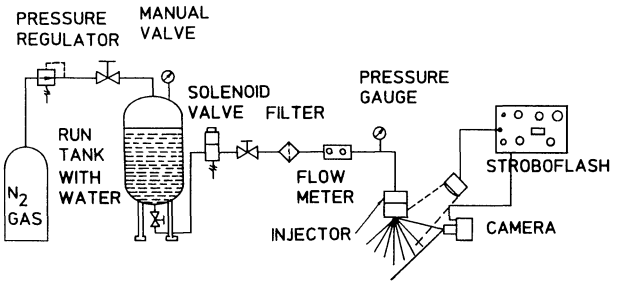

Fig. 4 Experimental setup.

nozzle assembly through a series of valves and a 2-μm filter. The swirled liquid sheets are formed in the ambient atmosphere, which is quiescent. The pressure upstream of the swirl nozzle is measured using a high-precision Bourden pressure gauge. Turbine flow meters are used for determining the flow rates, and these values are checked by collecting the spray over a given duration. The discharge coefficient of the orifices, Cd, is determined from the measured flow rates and pressure drop across the nozzle.

The thickness of the liquid sheet is determined from the experimentally measured value of Cd. Rizk and Lefebvre[7] have modified the theoretical expression relating Cd with the ratio of area of air core area to orifice area β to give

$$Cd = K_v\sqrt{\frac{(1-\beta)^3}{(1+\beta)}} \tag{2}$$

where K_v is the velocity coefficient that takes into account the flow losses in the nozzle. For a Simplex atomizer with tangential inlet ports, Rizk and Lefebvre[7] derive expressions for the film thickness. These could not be applied for the swirler generated flows in the present experiments because the flow losses are strongly influenced by the detailed configuration of the nozzle. However, over the small range of parameters during which transition of shape takes place, the change of the coefficient would be small. The value of β that gives the experimentally measured value of Cd is used for estimating the thickness of the liquid film at the exit of the orifice, h_0. The average liquid jet velocity u_0 is calculated from the measured flow rates and the estimated value of the film thickness.

The water injection velocities are varied to give variations over two orders of magnitude in the Reynolds number and Weber number of the liquid sheet. The liquid sheet is illuminated with a strobe flash. The half-crest value of the flash is 30 μs. The frequency of the dominant wave motion on the sheet is identified as the frequency of the strobe flash at which the maximum growth rate is observed. The integral multiples of this strobe frequency produce a clear picture of the wave motion; however, the growth rates are lower than the maximum value. The liquid sheet is photographed using a still camera with the flash from the strobe being operated in a single-pulse mode. The shape of the sheet, the divergence angle of the sheet at the exit of the orifice, and the amplitude of wave motion are determined using the enlarged photographs.

The accuracy of the flow measurements is 0.5%, whereas the accuracy of the pressure measurements is better than 0.3%. The measured frequencies of waves formed over the liquid sheets are accurate to 0.5 Hz.

Results and Discussions

Shape of the Sheet

Figure 5 gives the forces acting over a small element of the swirled liquid sheet of length dL, thickness h, and of arc length $r\,d\theta$ after it traverses a distance L from the orifice. The centrifugal forces F_1 and F_2 due to the meridian component of the axial velocity and tangential velocity, respectively, cause the sheet to diverge. The surface tension forces T_1 and T_2 due to the radius of the sheet, r, and the curvature along the meridian, R, tend to collapse the sheet. The inertial force I acts in the direction of the sheet, whereas the aerodynamic drag D acts in a direction opposite to the motion. The overall shape of the liquid sheet is decided by the relative magnitudes of the centrifugal, inertial drag, and the surface tension forces. Unlike the large tulip-shaped liquid sheets of water bells,[8] the injection velocities used in the swirled nozzles are significantly larger and the effect of gravity can be neglected. The liquid phase Weber number We_l, which is the ratio of the inertial and surface tension forces, is defined for the flow conditions at the exit of the orifice with the half-thickness of the liquid sheet, $h_0/2$ as the characteristic dimension and is given by

$$We_l = \rho_l h_0 u_0^2/2\sigma \tag{3}$$

As the inertial forces are proportional to the centrifugal forces, it is likely that We_l could be indicative of the shape of the liquid sheet formed.

The divergence angle of the sheet, α, at the exit of the orifice is plotted as a function of We_l in Fig. 6. The divergence angle is expressed in a nondimensional form with reference to the characteristic helix angle of the swirler, the area of cross section of the flow in the swirler, and the swirler and orifice diameters. It is observed that the divergence angle increases as We_l increases. This is due to the increased centrifugal and inertial forces at higher We_l, which arrest the collapse of the sheet by the surface tension and brings about an increase of α.

The different points in Fig. 6 correspond either to a tulip-bulb or a conical-shaped sheet and are indicated by shaded and open symbols, respectively. It is seen from Fig. 6 that values of We_l less than 140 always result in a tulip-shaped sheet, whereas when $We_l > 170$ a conical sheet is invariably formed. The transition from a tulip bulb to a conical diverging sheet, therefore, takes place for We_l between 140 and 170. The results are seen to be valid for all swirl numbers between 1.4 and 14.5 and orifice diameters between 1 and 10 mm for which the experiments are done.

The transition of the shape of the sheet can also be examined in terms of the Reynolds number. The Reynolds number of the liquid

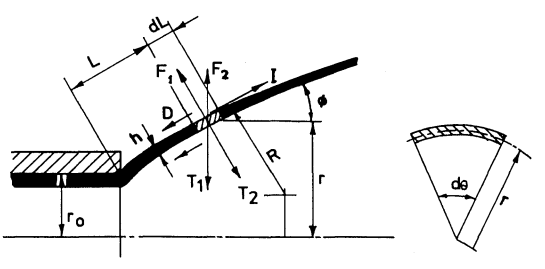

Fig. 5 Schematic of forces on an element of liquid sheet.

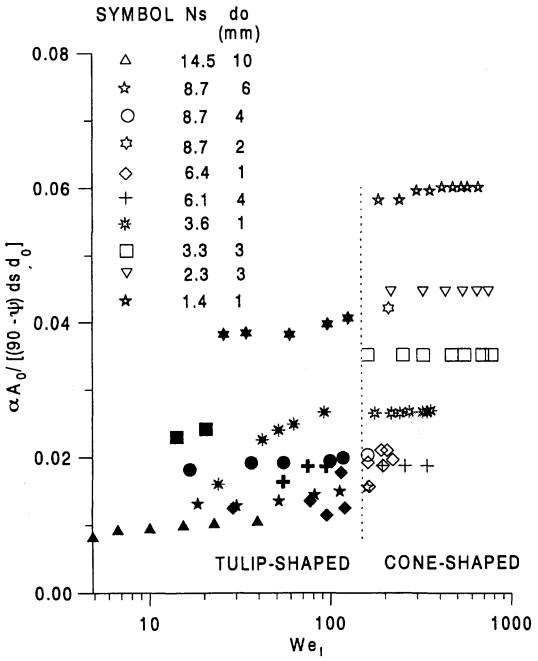

Fig. 6 Variation of divergence angle.

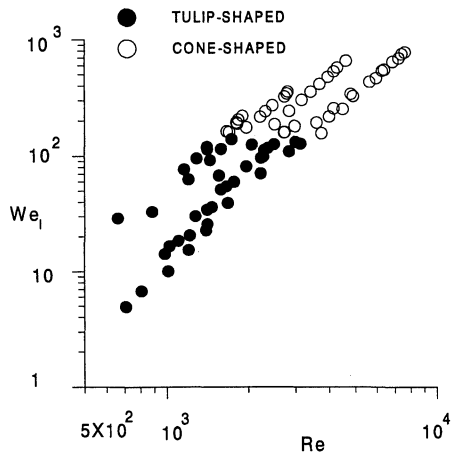

Fig. 7 Regimes of conical- and tulip-shaped sheets.

sheet is defined corresponding to the conditions at the exit of the orifice with the sheet thickness h_0 as the characteristic dimension.

$$Re_l = \rho_l h_0 u_0 / \mu \tag{4}$$

The range of Reynolds number in the experiments was between 400 and 100,000. The results of the different experiments, which gave either a conical sheet or a collapsed sheet, are plotted in Fig. 7 as a function of liquid Weber number and Reynolds number defined in Eq. 4. The filled symbols denote the tulip bulb whereas the open symbols show the conical-shaped sheet. It is seen that the tulip-shaped sheet and the conical divergent sheet coexist over a wide range of Reynolds number between 1200 and 3000. The transition in the shape of the sheet does not take place over a small range of Reynolds number as it does with Weber number. However, Fig. 7 shows that when $Re_l < 1200$ the sheet formed is always a tulip bulb whereas with $Re_l > 3000$ the sheet is a divergent cone.

The tangential velocity due to swirl also gives rise to centrifugal forces. The rapidly intensifying waves are seen to be present only along the length of the sheet (Fig. 1) without any trace of waves along the circumference. It is, therefore, unlikely that the tangential velocities would influence the transition of the shape. A swirl Weber number We_s is defined in terms of the tangential velocity at the exit of the orifice, v_{w0}, i.e., $We_s = \rho_l v_{w0}^2 h_0 / 2\sigma$, where v_{w0} is obtained from the conservation relations as $(1 - \beta) u_0 N_s / \beta^{1/2}$. The shape of the sheet is examined at different values of swirl Weber number in Fig. 8. It is seen that both the tulip bulb and the cone-shaped sheet

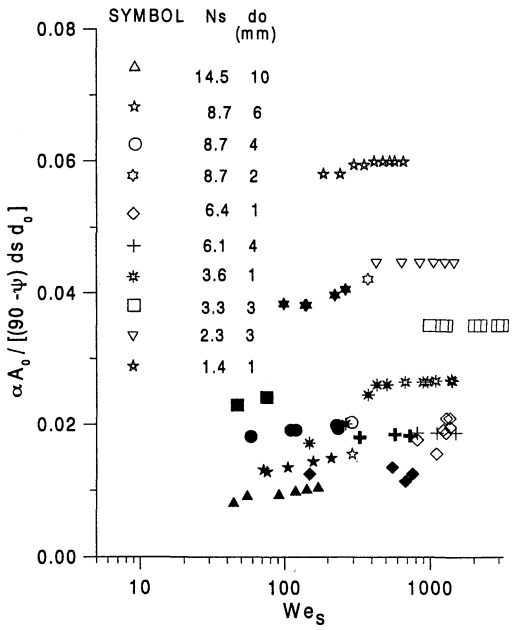

Fig. 8 Divergence angle of sheet at different swirl Weber number.

coexist over a wide range of swirl Weber number as expected. The change in the shape of the sheet for all values of swirl intensities is described only by the value of liquid Weber number exceeding about 150.

To understand the role of the turbulence on the change of the shape, the liquid sheets formed by varying the surface roughness of the 4-mm-diam orifice are examined. The average surface roughness values Ra of the orifice was varied between 0.5 and 12 μm. It was observed that, as the average surface roughness Ra of the orifice is increased, the surface texture of the sheet became more frothy compared to the translucent or glassy appearance observed at the lower Ra values of the orifice. The frothy surface is associated with turbulence in the jet. Figure 9 shows the translucent and turbulent frothy surface textures formed on the tulip bulb and the conical-shaped divergent sheets at $Ra = 1.2$, 4.5, and 12 μm, respectively. Though the tulip-shaped and the conical-shaped sheets are formed with the different surface textures, the change in the shape from a tulip to a cone occurred at about the same liquid Weber number of about 150. Also, no pronounced change in the wave growth pattern was discernible with changes in the frothing of the liquid sheet. The surface distortions due to turbulence in the flow do not accelerate or delay the formation of wave motion nor do they bring about a change in the Weber number at which the transition of the shape of the sheet takes place.

Wave Motion on Surface

The frequencies F corresponding to maximum growth of wave motion on the surface of the sheets are determined by synchronizing the frequency of the strobe flashes for the maximum wave growth on the sheet. The measured frequencies and maximum growth rates at different injection velocities are given in Figs. 10 and 11 for the 1- and 3-mm orifices with swirl numbers of 6.4 and 3.3, respectively. It is seen that the frequency and growth rate monotonically increase with Weber number. At the lower ranges of Weber number at which the tulip bulb is formed, there is no perceptible growth of wave motion on the sheets.

Disturbances are always present on the surface of the liquid sheets. It is seen that these disturbances are amplified at larger values of Weber number. The exponentially increasing growth rates for $We_l > 150$ contribute to the formation of the cone-shaped wavy sheets.

The observed dependence of frequencies and growth rates on liquid Weber number can be theoretically determined considering a flat liquid sheet moving at a mean velocity u_0 in the x direction and superimposing sinusoidal antisymmetric disturbances on it. These disturbances are assumed to evolve only along the sheet, without any transverse wave motion. The assumption is justifiable for modeling

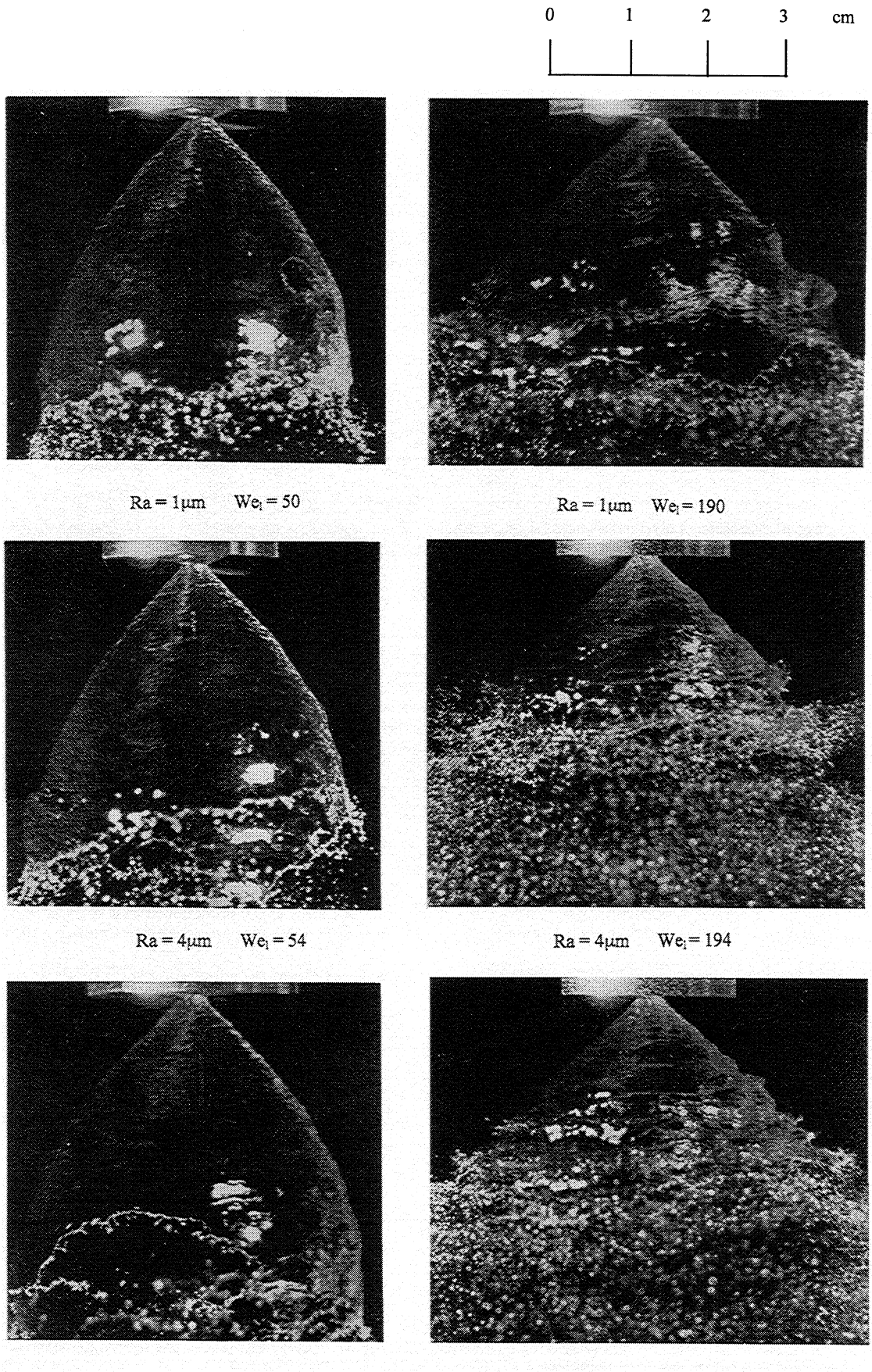

Fig. 9 Sheets formed at different surface roughness of the orifice.

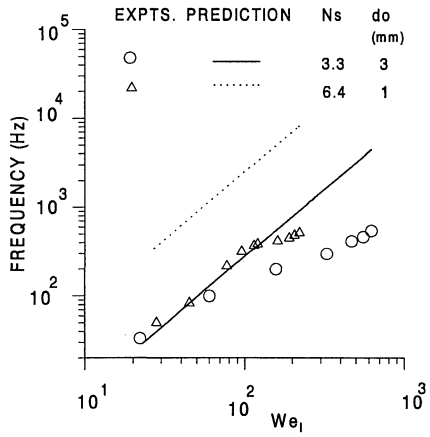

Fig. 10 Dependence of frequency on Weber number.

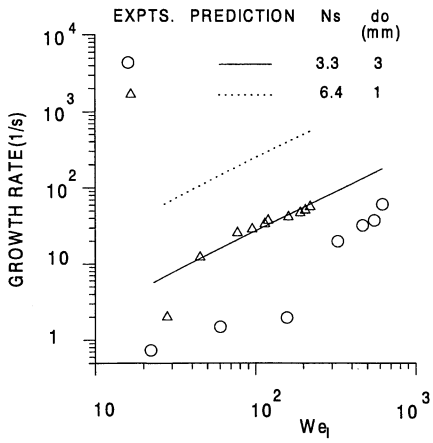

Fig. 11 Growth rate variations.

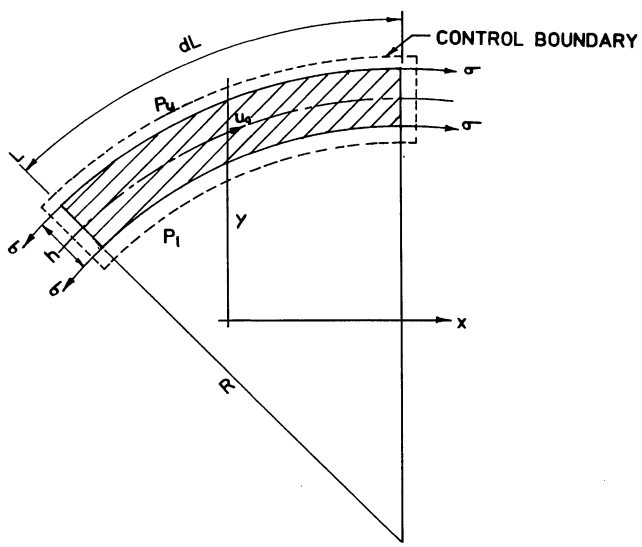

Fig. 12 Control volume of liquid sheet.

wave motion on swirled annular liquid sheets, based on experimental observations of Figs. 1 and 9, which show antisymmetric waves to grow mainly along the longitudinal axis without any trace of waves in the tangential direction. The dilation or symmetric wave modes are also not seen in the experiments. These would occur at negligibly small injection velocities wherein surface tension forces induce the instability. A control volume of an element of the liquid sheet of width dL and thickness h is shown in Fig. 12. The aerodynamic shear at the surface of the disturbed liquid sheet induces pressures P_u and P_l on the upper and lower sides of the liquid sheet. The longitudinal waves cause pressure fluctuations in the liquid sheet. Turbulent flow fluctuations in the liquid sheet are not considered.

The equation for momentum conservation along the x axis when applied to the control volume of Fig. 12 gives

$$\frac{\partial U}{\partial T} + U\frac{\partial U}{\partial X} = -\frac{\partial Cp}{\partial X} \tag{5}$$

The parameters in the Eq. (5) are nondimensional. The characteristic length and timescales are λ and λ/u_0, respectively.

The perturbation in the vertical velocity V' due to the disturbance can be expressed as the total derivative of the dimensionless interface displacement η of the liquid sheet in the y direction:

$$V' = \frac{\partial \eta}{\partial T} + \frac{\partial \eta}{\partial X} \tag{6}$$

where η can be assumed to have the form $\eta = \eta_0 \exp i(2\pi X - NT)$, η_0 being the initial amplitude and N the complex nondimensional frequency.

Expressing the values of U in terms of a steady value and a perturbation as

$$U = 1 + U' \tag{7}$$

and linearizing Eq. (5) for X momentum we get

$$\frac{\partial U'}{\partial T} + \frac{\partial U'}{\partial X} = \frac{\partial}{\partial X} Cp \tag{8}$$

The value of Cp in Eq. (8) is calculated following the procedure of Rangel and Sirignano.[4] This consists of solving the Laplace equation for the gas and liquid phases along with the kinematic condition given by Eq. (6) and the condition that $V' = 0$ at $Y = \pm\infty$. The velocity potentials for the gas and liquid are determined for the antisymmetric wave motion and are substituted in the linearized X momentum Eq. (8) to get the values of Cp for the liquid and gas, respectively. These are used in the equation for dynamic balance between the surface tension and pressure given by Rangel and Sirignano[4]:

$$Cp_{l,u} - Cp_{g,u} = H/(2WeR) \tag{9}$$

to solve for the nondimensional frequency, which is obtained as

$$N = \frac{2\pi \tanh Z \pm 2\pi\sqrt{\tanh^2 Z - (\rho + \tanh Z)(\tanh^2 Z - W\rho/[1+\rho])}}{(\rho + \tanh Z)} \tag{10}$$

where

$$Z = We_l W\rho/(1+\rho) \tag{11}$$

and W, the nondimensional wave number, is

$$W = 2\pi\sigma(1+\rho)/(\rho_g u_0^2 \lambda) \tag{12}$$

The frequency and growth rate are given by the real and imaginary part of N in Eq. (10). The value of W that gives maximum growth rate is calculated and the corresponding frequency determined. The dimensional frequencies and growth rates are found by multiplying the nondimensional values by λ/u_0, and λ is obtained from the value of W by specifying values of u_0 and h_0 determined from the experimental Cd measurements. The density ratio ρ of 0.001 corresponding to air and water is used. The calculated values of frequencies and growth rates for the 1- and 3-mm orifice are compared with the experimental measurements in Figs. 10 and 11.

The predicted values of frequencies and growth rates are observed to be higher than the experimental measurements. Note that the perturbations in the tangential direction are not considered in the predictions. Panchagnula et al.[9] show a decrease in growth rate with increase of tangential velocities. The neglect of the transverse transport properties may be responsible for the overpredictions. The estimated value of h_0 based on Cd measurements would also influence the predictions of frequencies and growth rates. However, it is seen that both theory and experiments show an exponential growth of waves as the liquid Weber number increases. The significantly larger values of growth rates at higher values of liquid Weber number, exceeding about 150, result in rapid growth of wave motion and the formation of a wave-dominated cone-shaped sheet.

Linear Stability Analysis

A linear analysis is carried out to determine the stability of the liquid sheet and the existence of a threshold Weber number at which the sheet changes from a tulip shape to a conical wave-dominated shape. Figure 5 shows the forces on an element of the liquid sheet of width dL, thickness h, and arc length $r\,d\theta$. Neglecting the weight of the sheet as being small compared to the inertial forces and equating the forces normal and parallel to the sheet, we get

$$F_1 + F_2 \cos\phi = T_1 + T_2 \cos\phi \tag{13}$$

$$I = D - F_2 \sin\phi + T_2 \sin\phi \tag{14}$$

where ϕ denotes the angle between the sheet and the axis of the orifice. Substituting the values of F_1, F_2, T_1, T_2, I, and D for the element dL in Eqs. (13) and (14), we get

$$\rho_l h\,dL r\,d\theta\left[u^2/R + (v_w^2/r)\cos\phi\right] = dL r\,d\theta[2\sigma/R + (2\sigma/r)\cos\phi] \tag{15}$$

$$\rho_l h\,dL r\,d\theta u\frac{du}{dL} = C_D\frac{\rho_g u^2}{2}(2\,dL r\,d\theta) - \rho_l(hr\,d\theta\,dL)v_w^2\sin\phi + \frac{2\sigma}{r}dL r\,d\theta\sin\phi \tag{16}$$

Simplifying Eqs. (15) and (16) and noting that the curvature along the meridian section, $1/R$, is given by $(-d\varphi/dL)$ (Ref. 8), the following equations are obtained:

$$\frac{d\phi}{dL} = -(\cos\phi/r)\{[\rho_l h v_w^2/2\sigma - 1]/[1 - \rho_l h u^2/2\sigma]\} \tag{17}$$

$$u\frac{du}{dL} = (2/\rho_l h)[\sigma\sin\phi/r + C_D\rho_g u^2/2] - v_w^2\sin\phi/r \tag{18}$$

Substituting the mass conservation relation $h_0 r_0 u_0 = hru$ and the conservation of angular momentum for tangential velocities $v_w r = v_{w0} r_0$, Eqs. (17) and (18) are simplified to give the following in the immediate vicinity of the orifice ($r \to r_0$):

$$\frac{d\phi}{d\xi} = -\cos\phi\frac{[(We_l S_w^2/U) - 1]}{[1 - (We_l U)]} \tag{19}$$

$$\frac{dU}{d\xi} = C_D\frac{\rho_g}{\rho_l}\left[\frac{U^2}{h_0/r_0}\right] + \sin\phi/We_l - \sin\phi S_w^2/U \tag{20}$$

where the parameters are written in nondimensional form as

$$U = u/u_0, \qquad S_w = v_{w0}/u_0, \qquad \xi = L/r_0 \tag{21}$$

Equations (19) and (20) are a set of autonomous partial differential equations that describe the evolution of the angle ϕ and the nondimensional velocity U near the orifice. The form of the equations is

$$\frac{d\phi}{d\xi} = f(\phi, U) \tag{22}$$

$$\frac{dU}{d\xi} = g(\phi, U) \tag{23}$$

Because the differential equations (19) and (20) are autonomous, it is possible to investigate the changes in ϕ and U about their stationary points using linear stability analysis similar to that of Uppal et al.[10] The stationary points of ϕ and U are represented by ϕ^* and U^* and are given by

$$\frac{d\phi}{d\xi} = f(\phi^*, U^*) = 0 \tag{24}$$

$$\frac{dU}{d\xi} = g(\phi^*, U^*) = 0 \tag{25}$$

The following matrix A is defined following Uppal et al.[10] for investigating the stability about ϕ^* and U^*:

$$A = \begin{bmatrix} \left(\frac{\partial f}{\partial\phi}\right)_{\phi^*,U^*} & \left(\frac{\partial f}{\partial U}\right)_{\phi^*,U^*} \\ \left(\frac{\partial g}{\partial\phi}\right)_{\phi^*,U^*} & \left(\frac{\partial g}{\partial U}\right)_{\phi^*,U^*} \end{bmatrix} \tag{26}$$

When the trace of matrix A is such that tr $A > 0$, the stationary points described by Eqs. (19) and (20) would be unstable provided the values of the determinant of matrix A are less than or greater than zero.[10] The instability then is either aperiodic or an unstable node or focus. The states around the stationary points would then exponentially grow with time.

The matrix A for the governing equations (19) and (20) reduces to

$$\begin{bmatrix} 0 & \{-\cos\phi^* We_l(-1 - S_w^2/U^{*2} + 2We_l Sw^2/U^*)/(1 - We_l U^*)^2\} \\ \{\cos\phi^*(1/We_l - S_w^2/U^*)\} & \{C_D(\rho_g/\rho_l)(2U^*/[h_0/r_0]) + \sin\phi^* S_w^2/U^{*2}\} \end{bmatrix} \tag{27}$$

The trace of the preceding matrix is given at the stationary points by

$$\text{tr } A = \{C_D(\rho_g/\rho_l)(2U^*/[h_0/r_0]) + \sin\phi^* S_w^2/U^{*2}\} \tag{28}$$

and is always positive. It shows that a higher ambient density ρ_g, a lower sheet thickness h_0, or a larger orifice radius r_0 have influence similar to higher swirl ratio or higher drag coefficient. A denser gas will have about the same effect on a thicker sheet as does a lower density gas on a thinner sheet. This is a physically observed phenomenon.

The determinant of matrix A is given by

$$\det A = \{\cos^2\phi^* We_l(2We_l Sw^2/U^* - 1 - S_w^2/U^{*2}) \times (1/We_l - S_w^2/U^*)/(1 - We_l U^*)^2\} \tag{29}$$

and is either positive or negative depending on the values of liquid Weber number and S_w. Because tr $A > 0$ and det $A > 0$ or < 0, the swirled liquid sheet is unstable for all values of liquid Weber number and S_w. Disturbances would, therefore, grow on the liquid sheet for all of the values of liquid Weber number. However, the growth rate of waves, obtained in the predictions and measured in experiments, is much larger for Weber number exceeding about 150. This leads to rapid intensification of wave motion for liquid Weber number exceeding about 150 and the transition from the tulip-shaped sheet to the wavy cone-shaped sheet.

Conclusions

Experiments with swirled annular water sheets show that the swirled liquid sheets change their characteristic shape from a tulip bulb to a cone-shaped wavy sheet when the liquid phase Weber number is greater than about 150. A tulip-shaped bulbous sheet, formed without significant wave motion on it at smaller values of Weber number, does not significantly amplify the wave motion unlike the cone-shaped sheets.

The frequency and growth rate of the waves on the liquid sheet increase with Weber number, and the experimental variations are confirmed by a linear theory. The predicted values of frequencies and growth rates, however, are higher than the experimentally measured values. It is the enhanced rate of growth of the amplitude of wave motion for Weber number greater than about 150 that leads to the formation of a wavy cone-shaped sheet. Variations of the intensity of turbulence in the flow do not influence the wave frequencies and the transition from the tulip-shaped sheet to the cone-shaped sheet. The transition in the shape of the sheet takes place over a wide range of Reynolds number and swirl Weber number.

A linear stability analysis brings out the importance of drag coefficients, ambient gas densities, thickness of the liquid sheet, swirl intensities, and radius of the orifice on the sheet stability. It is seen that a swirled liquid sheet is unstable at all Weber numbers and swirl

intensities. When the amplification of the waves on the surface of the intrinsically unstable liquid sheet is small, a relatively smooth tulip-shaped sheet is formed. If not small, the larger amplification of waves, obtained at higher values of Weber number, causes a significant buildup of wave motion, leading to disintegration of the annular swirled liquid sheet in the form of a conical wavy sheet.

Acknowledgments

The comments of the reviewers have been useful for revising the manuscript and are gratefully acknowledged.

References

[1]Cheuch, S., "Numerical Simulation of Nonswirling and Swirling Annular Liquid Sheets," *AIAA Journal*, Vol. 31, No. 6, 1993, pp. 1022–1027.

[2]Ramamurthi, K., and Tharakan, T. J., "Experimental Study of Liquid Sheets Formed in Coaxial Swirl Injectors," *Journal of Propulsion and Power*, Vol. 11, No. 6, 1995, pp. 1103–1109.

[3]Faeth, G. M., "Structure, Breakup and Turbulence Interactions in Sprays," *Atomization and Sprays 2000*, edited by N. F. Chigier, Proceedings of Workshop Sponsored by National Science Foundation, Carnegie Mellon Univ., Pittsburgh, PA, 1991, pp. 27–39.

[4]Rangel, R. H., and Sirignano, W. A., "The Linear and Nonlinear Instability of a Fluid Sheet," *Physics of Fluids*, Vol. 3, No. 10, pp. 2392–2400.

[5]Mansour, A., and Chigier, N. A., "Effect of Turbulence on the Stability of Liquid Jets and the Resulting Droplet Size Distributions," *Atomization and Sprays*, Vol. 4, No. 5, 1994, pp. 583–604.

[6]Ruiz, F., and Chigier, N. A., "Design and Uncertainty Analysis of a Series of Experiments in Seven Variables," *Journal of Fluids Engineering*, Vol. 112, No. 1, 1990, pp. 96–114.

[7]Rizk, N. K., and Lefebvre, A. H., "Internal Flow Characteristics of Simplex Swirl Atomizers," *Journal of Propulsion and Power*, Vol. 1, No. 3, 1985, pp. 193–199.

[8]Taylor, G. I., "The Dynamics of Thin Sheets of Fluid. I. Water Bells," *Proceedings of Royal Society of London, Series A: Mathematical and Physical Sciences*, Vol. 25, No. 253, 1959, pp. 289–295.

[9]Panchagnula, M. V., Sojka, P. V., and Santangelo, P. J., "On the Three Dimensional Instability of a Swirling Annular, Inviscid Liquid Sheet Subject to Unequal Gas Velocities," *Physics of Fluids*, Vol. 8, No. 12, 1996, pp. 3300–3312.

[10]Uppal, A., Ray, W. H., and Poore, A. B., "On the Dynamic Behavior of Continuous Stirred Tank Reactors," *Chemical Engineering Science*, Vol. 29, No. 4, 1974, pp. 967–985.

G. M. Faeth
Editor-in-Chief